JMEPEG (2021) 30:9412–9425
https://doi.org/10.1007/s11665-021-06084-6

©ASM International
1059-9495/$19.00

The Mechanical Properties and Microstructure of Nanostructured Cu with a Flexible Random Distribution of Multimodal Grain Size Prepared by a Combination of Electrodeposition and Recrystallization Annealing

Linbo Liu, Xixun Shen, Chengwei Deng, Tao Wang, Hong Yun, and Qunjie Xu

Submitted: 19 May 2021 / Revised: 6 July 2021 / Accepted: 16 July 2021 / Published online: 19 August 2021

A bulk nanostructured (NS) Cu with a flexible random distribution of multimodal grain size ranging from 1.12 μm to 30 nm was fabricated here by annealing a pre-designed heterogeneous layered structure Cu template fabricated by electrodeposition where the small grains with average grain size of about 40 nm and a large grain size with near micron scale distribute alternately according to the layer thickness ratio of about 4:1 along the deposition direction. Such a heterogeneous NS Cu exhibits a remarkable large strain hardening ability in tensile deformation, which results in a superior combination of high ductility of elongation to failure of near 40% and moderated strength of yield strength of about 470 MPa. Several strengthening effects brought by such a heterostructure, including producing more effective dislocation activity, the inhibition of local plastic flow and the release of local stress concentration, have been suggested to contribute to a more durable strain hardening ability and excellent mechanical properties of NS Cu. In addition, the morphology of fracture and deformation surface is captured to analyze the difference in the mechanical behavior of the NS Cu with random distribution of multimodal grain size by comparing with other structure Cu.

Keywords electrodeposition, multimodal grain size, mechanical properties, nanocrystalline metals, recrystallization annealing

1. Introduction

Nanostructured metals have potential applications in the areas of reinforced coatings and structural materials because this new class of materials exhibits strength and hardness several times higher than traditional coarse-grained counterparts. However, such expected potential applications are limited because the high-strength NS materials often exhibit plastic instability and premature yielding during deformation (Ref 1), which results in a disappointingly low plasticity. Therefore, how to optimize the combination of strength and plasticity of the NS material has become a research hotspot and has attracted the attention of many researchers in recent years. Extensive experiments and simulations have suggested that low plasticity is attributed to the lack of effective work hardening ability due to the lack of effective dislocation activity inside such small-scale grains. The challenge posed by the inherent low ductility of nanocrystalline (NC) metals has prompted researchers to increase the ductility by tailoring an uneven microstructure with a multimodal or bimodal grain size distribution in recent years. For example, Wang et al. fabricated a NS Cu with a bimodal grain size distribution of micrometer-sized grains embedded inside a matrix of nano-sized grains by the combination of cryogenic rolling and thermomechanical treatment. The bimodal structural Cu with a mixture of large grain with micron-level and ultrafine grains (< 300 nm) has a high tensile ductility with a uniform elongation of about 30% and a moderate ultimate tensile strength (UTS) of about 400 MPa (Ref 2). Takahiro Mineta et al. also fabricated NC Ag with a bimodal microstructure composed of a few equiaxed grains with average grains sizes of about 86.0 nm and ultrafine grains with average grains sizes of less than 500 nm by a combination of spark plasma sintering and arc plasma method. The bimodal-structured Ag produced an ultimate tensile strength of approximately 270 MPa combined with a uniform elongation of more than 30%, which was 1.4 times larger than that of the homogeneous coarse-grained counterparts (Ref 3). Lu et al. constructed a bulk coarse-grained (CG) pure Cu by surface mechanical grinding treatment with a gradient grain size distribution from 20 nm to 20 μm from surface to inside along the cross section by surface mechanical grinding treatment. Compared with the coarse-grained Cu with a uniform structure, the gradient structure Cu can produce several times higher strength and plasticity (Ref 4). These studies illuminate that tailoring the inhomogeneous microstructure with the bimodal and multimodal grain size distribution by incorporating large size grains into the NC matrix is an effective way to improve the plasticity of NS materials. From the perspective of the practical application of engineering materials, if such a strategy

Linbo Liu, Xixun Shen, Hong Yun, and **Qunjie Xu**, Shanghai Key Laboratory of Materials Protection and Advanced Materials in Electric Power, Shanghai Engineering Research Center of Energy-Saving in Heat Exchange Systems, Shanghai University of Electric Power, Shanghai 200090, People's Republic of China; and **Chengwei Deng** and **Tao Wang**, Space Power Technology State Key Laboratory, Shanghai Institute of Space Power-Sources, Shanghai 200245, People's Republic of China. Contact e-mails: shenxixun@shiep.edu.cn and xuqunjie@shiep.edu.cn.

is to be applied in practice, the effective and controllable preparation of such heterogeneous structure becomes particularly important. Although the above methods can be used to prepare such heterogeneous NS materials, these methods were not used to flexibly control the proportion and distribution of heterogeneous structures and the heterogeneous structure tailored by these methods is random in optimizing properties of NS material. In addition, these processes also have limitations such as complex processes, poor operability in practical application, which cannot meet the actual requirements of large-scale production.

Electrodeposition is a process based on the bottom-up stacking of atoms. Due to its simple process and easy operation, it has been widely used in many industrial fields for surface treatment and manufacturing functionalized coating and structural materials. Furthermore, the structure of coating can also be flexibly controlled by simple changing process parameters and solution composition during electrodeposition. This process has been popularly used to produce the high-quality NS materials with uniform structure in the past 30 years. Recently, we use the electrodeposition method to design the layered heterogeneous NS Cu and NS Ni with regular alternate growth of nanocrystals and ultrafine crystals flexibly by adjusting the process parameters such as current and voltage (Ref 5, 6). Compared with homogeneous NS components, layer structural materials we designed do have a significant improvement in plastic deformation capability, but the improvement is not as large as expected, which may be related to the case that in such a layered heterogeneous NS formed by the periodic alternately stacking of the large-sized grain layer and NC layer in a mechanical abrupt manner, the large-sized grain layer mechanically arranged in the NC matrix may not be able to effectively coordinate the plastic deformation of internal NC layer. This may mean that in the process of heterostructure design, if the large-sized grains and the small-sized grains can be flexibly and naturally distributed in the matrix with each other, the large grains in such a heterostructure can more effectively coordinate the deformation of small grains and a more optimized mechanical properties may be expected. This analysis prompted us to produce a new design idea that if the layered heterogeneous NS material we designed replaces the traditional homogeneous structure material as the template before heat treatment, it may be expected to construct heterogeneous structural materials where multi-stage microstructures with different grain size are distributed evenly and flexibly with each other.

Based on such a design idea, here, a layered NS copper template with the alternating growth of the large-sized grain layer and nano-sized grain layer was first prepared by electrodeposition and then subsequently was followed by an annealing treatment to construct this expected heterogeneous structural materials with flexible random distribution of multimodal grain size. Transmission electron microscopy and x-ray diffraction were employed to analyze the heterogeneous structure. Uniaxial tensile tests were used to investigate the mechanical behavior of the heterogeneous NS Cu with multimodal grain distribution and other structure Cu. Fracture and deformation surfaces of Cu samples were also provided for further analysis of the fracture behavior of Cu samples with different structures.

2. Experimental Procedure

The bulk dense NS Cu with multimodal grain size distribution was fabricated by annealing an electrodeposited Cu with a layered structure template where the small grain-sized layer with a mean grain size of about 40 nm and the large grain-sized layer with a grain size of near micron scale alternate according to the layer thickness ratio of about 4:1 along the deposition direction. The bulk layered structure Cu (LS-Cu) was prepared by periodical changing current density during electrodeposition from an aqueous bath that consists of copper sulfate, copper chloride, sulfuric acid and other additives at room temperature. Here, two kinds of current density, that is, 1.5 A/dm^2 for 16 min and 10 A/dm^2 for 1 min, were designed to prepare the LS-Cu with the layer thickness ratio of near 4:1 and detailed preparation process of electroplating can refer to our previously reported literature (Ref 5, 6). The as-deposited LS-Cu was kept at a temperature of 200 °C for 10 min under a protective nitrogen atmosphere and then cooled to room temperature in the furnace, and finally, a NS Cu sample with multimodal grain size distribution was obtained. For the convenience of statement, the ALS-Cu is used as the abbreviation of this NS Cu with multimodal grain size distribution in the following statements. In addition, three corresponding monolithic samples including the ultrafine grain Cu (UFG-Cu) and monolithic nano grain Cu (NG-Cu) and coarse grain Cu (CG-Cu) with homogeneous structure were also fabricated as references for the comparison of mechanical properties. Chemical analysis from inductively coupled plasma atomic emission spectrometry (ICP-AES, Plasma/1000) and Carbon/Sulfur determinator (CS-20) showed that as-deposited Cu samples all have a similar high purity of about 99.95 wt.% and the main impurities of 120 ppm S, 310 ppm C. These trace impurities may be introduced by the decomposition of used additives during electrodeposition and other chemicals. The crystallographic structure of as-deposited Cu samples with different microstructure was investigated by using the x-ray diffractometer (XRD, Bruker D8) with a Cu Kα radiation (0.154178 nm) operated at 40 kV and 40 mA over scanning angle range of 10°-80° with a scanning step size of 0.01°. Wire-electrode discharge machines were employed to prepare the dog bone-shaped tensile specimens with a gauge length of 8 mm and cross section of 2.5×0.5 mm^2. To truly display the essential tensile properties of these heterogeneous and homogeneous samples, these samples were polished to a mirror-like finish surface to remove surface defects such as microcracks and pits before tension. The effect of heat treatment on grain morphology and grain size was analyzed by transmission electron microscope (TEM, a JEM-2100F). The uniaxial tensions were conducted on the Electro-Mechanical Material Testing System (UTM5105SYXL) at a strain rate of 4.17×10^{-2} s^{-1}. Here, in order to avoid the experimental deviation that may be caused by a single sample, three parallel samples for each type of copper were used to perform tensile tests. The morphology from the fracture surface and deformation surface was also observed by using the scanning electron microscope (SEM, JSM-5600).

3. Result and Discussion

In order to analyze the microstructure of the layered sample before and after heat treatment, a bright-field TEM observation of the LS-Cu samples and ALS-Cu samples was also made and the corresponding result is shown in Fig. 1 and 2, respectively. For comparison, the bright-field TEM images of the monolithic UFG/NG-Cu samples were also provided and shown in Fig. 3. The bright-field TEM image of as-deposited LS-Cu prepared by intermittent changing two current density, as shown in Fig. 1(a), displays a clear layered structure alternatively composed of two different microstructures corresponding to two current density. The deposited layer corresponding to the low current density exhibits a very fine NC structure. Furthermore, it can be seen from the local magnification image of the NG layer shown in Fig. 1(b) that crystal grains in the NG layer formed at low current density exhibit obvious columnar growth characteristics. In order to further understand the microstructure of the NG layer, the grain size distribution of the nanocrystal grain along the radial and axial direction is statistically analyzed and the corresponding results are shown in Fig. 1(f). As shown in Fig. 1(f), the nanocrystal grains with a axial length of about 60-230 nm and a radial width of about 15-80 nm preferentially grow regularly along the electrodeposition direction. The selected diffraction pattern shown in the inset of Fig. 1b also shows an obvious diffraction ring, which further implies that the deposited layer obtained at low current density is composed of polycrystalline nanocrystals. Recently, it has been implied from many experiments (Ref 7-9) that during the electrodeposition process, a more uniform and fine grain structure under high current density can be obtained because the applied high current density is more beneficial for the metal ion reduction and then increases the nucleation rate of metal atoms. However, here, it can be seen from Fig. 1(c) that the microstructure of the deposited sublayer corresponding to high current density in present layer structure is not further refined, and inversely, a microstructure with an approximately micron-sized grain with some stacking faults marked by the white arrow was observed. Such an interesting phenomenon that the microstructure of the deposited layer becomes larger with the increase of current density observed in the layered NS coatings can also be further proved by the homogeneous structure deposits obtained under their corresponding two single current density. It can be observed from Fig. 3 that the microstructure of monolithic deposited samples attained under 1.5 A/dm^2 shows a typical equiaxed grains with a narrow grain size distribution ranging from 20 to 70 nm and the average grain size of NC Cu is 40 nm. While for the monolithic deposited samples attained under 10 A/dm^2, as shown in Fig. 3, a microstructure with the irregular polygonal micron-sized grains and some stacking faults can be observed. Obviously, the microstructure of the sample attained under two single current density is consistent with that of the NC layer and UFG layer of the LS-Cu. For heterostructure materials, a good connection between interfaces is very important to obtain a considerable mechanical performance. Here, it can be seen from the TEM image at the interface of the layered structure shown in Fig. 1(a) that there are no defects such as voids in the interface area corresponding to the alternating layers formed at the two current densities. In addition, considering that there may be differences in structural defects such as dislocation density and crystal lattice within the microstructure obtained under the two current densities, the local high-resolution and the corresponding inverse FFT (fast Fourier Transform) analysis from the micro-grain layer region and the NC region were also done and the corresponding results are shown in Fig. 1(d) and (e), respectively. It can be revealed by the high-resolution image and Fourier filtering image shown in Fig. 1(d) that the crystal lattice of NC layer attained under the low current density presents an ordered lattice arrangements in which only small amount of edge dislocations are detected as marked by the symbol "T." However, for the micron-level crystal grain layer formed at high current density, as shown in Fig. 1e, the crystal lattice displayed by high-resolution does not show a regular parallel shape like the crystal lattice in the NC area, but shows a clear meandering shape. In addition, it can also be further observed from the partial enlarged high-resolution view shown in Fig. 1(e) that there are many substructures marked by the white arrow in this large-grained layer with a near micrometer scale. The Fourier filtered image shows a wave-like morphology with severe distortion, which can imply there is a number of dislocations within their lattice (Ref 10). The existence of a large number of structural defects may be the reason why the diffraction pattern of the large-grained layer shown in the inset in Fig. 1(c) exhibits the diffraction spots with obvious phantoms like comet tails. The present results show that the current density has a significant effect on the microstructure of coating. Such structural defects in the deposited layer formed under the high current density are likely to be related to the growth behavior that a large number of reduced copper atoms cannot be effectively stacked in the right way (that is, in the right atomic stacking position) due to mutual competition and constraint in the process of high-speed electrodeposition. The microstructure of layered copper after heat treatment has changed significantly. The TEM image of ALS-Cu samples is shown in Fig. 2(a), where the region marked the letter "A" and that marked the letter "B" distinguished by green dotted lines correspond to the NG layer and the UFG layer of LS sample, respectively. From the area marked by the letter "A" in Fig. 2(b), it can be observed that the microstructure characteristics of the columnar growth nanocrystals that originally appeared in the layered structure have completely disappeared after heat treatment and on the contrary, the equiaxed polygonal submicron crystal grains with grain size spanning from 250 to 791 nm form. Moreover, it can be further observed from the enlarged image that in addition to the formation of equiaxed submicron crystal grains, there are still a considerable number of nanocrystals that have not yet grown up around these equiaxed submicron grains after the heat treatment, as shown by arrow in Fig. 2(b). The heterogeneous distribution of grain size after the heat treatment of NC layer should be related to the abnormal anisotropic growth of grain during the heat treatment. It is well known that in polycrystalline materials, the growth of grains is achieved by the grain boundary migration companied by merging with neighboring grains. It has been suggested from the Bai's study that non-equilibrium grain boundary structure with structural defects such as dislocation and stress concentration often provide a large driving stress for the mobility of grain boundaries (Ref 11). It is conceivable that the deviation of the structure of the grain boundaries in a NC material from the equilibrium boundary structure is inhomogeneous throughout the bulk sample. Thus, in such an environment with inhomogeneous grain boundary structure, some grains with high-energy non-equilibrium grain boundary will grow preferentially by the rapid grain boundary migration or local adjustment

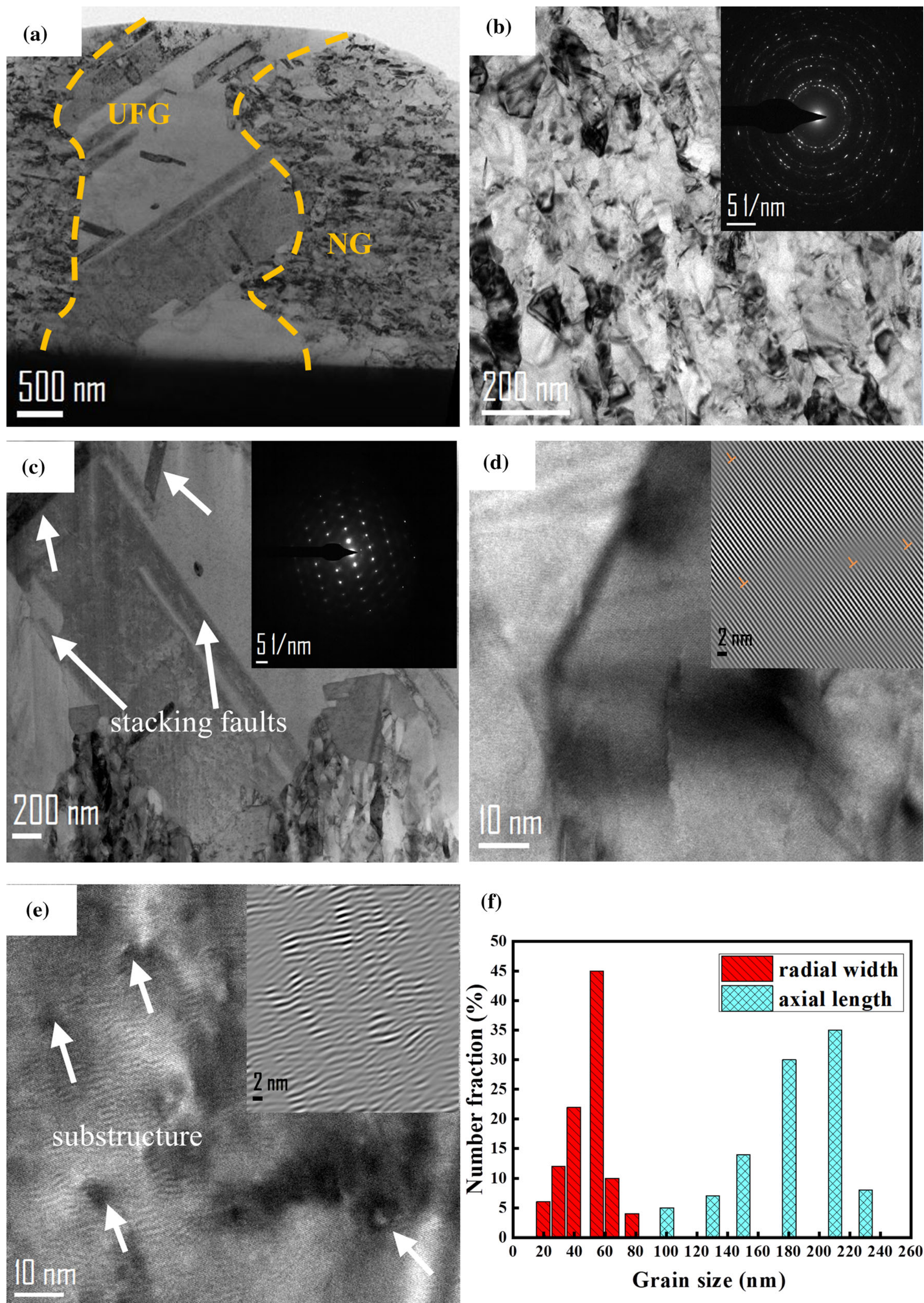

Fig. 1 Bright-field TEM images of the LS-Cu: (a) The low magnification image of the LS-Cu containing NG layer and UFG layer; (b) The local magnification image of the NG layer and (c) The local magnification image of the UFG layer; (d-e) High-resolution TEM images of the NG layer and UFG layer; (f) The narrow grain size distribution image corresponding to the NG layer of the LS-Cu

combined with nearby grains driven by external heat source, which results in formation of microstructure with bimodal grain size distribution after heat treatment. However, unlike the coarsening behavior of NC layer after heat treatment, the inner crystal grains from microcrystalline layer did not grow further after the heat treatment and inversely, as shown in the area

Fig. 2 Bright-field TEM images of the ALS-Cu: (a) The low magnification image of the ALS-Cu. (b) The local magnification image of A region of the ALS-Cu corresponding to the NG layer of the LS-Cu and (c) The local magnification image of B region of the ALS-Cu corresponding to the UFG layer of the LS-Cu. (d) The multimodal grain size distribution images of the ALS-Cu

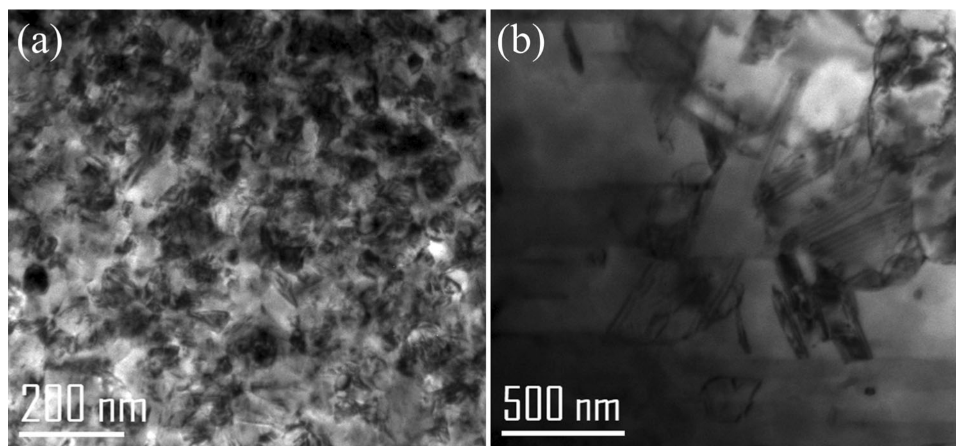

Fig. 3 Bright-field TEM images of the monolithic NG-Cu and UFG-Cu

marked by the white letter "B," the microstructure was evidently refined and equiaxed grains with an average grain size of approximately 600 nm formed in the original the large grain-sized area with nearly micron grain size. The grain refinement should be related to the large number of dislocation defects in the microcrystalline area inside the layered structure.

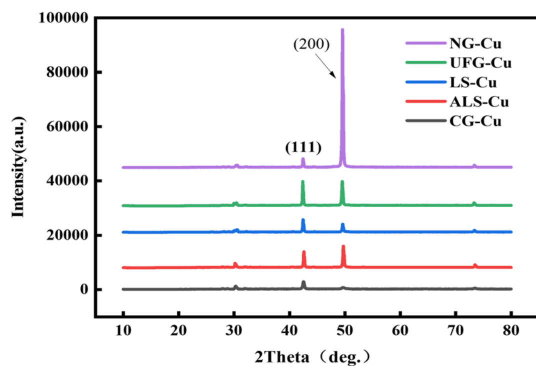

Fig. 4 The XRD patterns of the NG-Cu, UFG-Cu, LS-Cu, ALS-Cu, and CG-Cu

The existence of a large number of defects in the matrix provides effective nucleation points for the nucleation of recrystallized grains in the annealing process (Ref 12), which results in grain refinement. In addition to equiaxed crystals with submicron size, some growth twins with a radial size of about 40-145 nm and an axial size of about 250-740 nm were also observed in the original large-grained region after the annealing, as shown by the arrows in Fig. 2(c). The corresponding diffraction pattern of these twins is shown in the inset in Fig.2(c), where double sets of diffraction spots representing twin structure were exhibited. Such growth twins have been widely reported in previous studies on the heat-treated copper (Ref 13-15). Obviously, here, a heterostructure structure with multi-stage grain size distribution is finally obtained by heat treatment of this layered structure. In order to clearly illustrate the heterostructure with multi-scale grain size distribution, the grain size in the ALS-Cu is also systematically counted and the corresponding results are shown in Fig. 2(d). It can be seen from Fig. 2(d) that the ALS-Cu shows a very wide grain size distribution with the grain size spanning from 30 nm to 1.2 µm. The present study illuminates that this method of pre-designed a layered structure template accompanied by subsequent heat treatment is an effective method for preparing heterostructure with a flexible random distribution of multimodal grain size distribution.

Figure 4 shows the XRD patterns of the NG-Cu, UFG-Cu, LS-Cu, ALS-Cu and CG-Cu. It can be seen from Fig. 4 that five Cu samples all show a single diffraction pattern of a face-centered cubic structure with three typical diffraction peaks corresponding to the crystallographic plane (111) at $2\theta = 43.316°$, (200) at $2\theta = 50.448°$ and (220) at $2\theta = 74.124°$, but they have significantly different diffraction peak intensities, which implies there are significant differences in the preferred growth orientations. The preferred orientation of five Cu samples can be determined by quantitatively comparing the peak ratios of diffraction intensity of their two main diffraction peaks (111) and (200) and that of isotropic polycrystalline Cu. The calculated ratios of diffraction intensity of the diffraction peak (111) and (200) for fives Cu samples are summarized in Table 1, where a ratio of diffraction intensity for isotropic polycrystalline Cu is also provided for comparison. It can be seen from Table 1 that the ratio of the diffraction intensity of I(111)/I(200) for the monolithic NG-Cu prepared at low current density of 1.5 A/dm^2 is calculated to be about 3.85, which is remarkably larger than that (about 2.13) of isotropic polycrystalline Cu (Ref 16). This means that the monolithic NG-Cu holds a (111) preferred growth texture. For the

Table 1 **The calculated ratios of diffraction intensity of the diffraction peak (111) and (200) for five samples**

Sample	NG-Cu	UFG-Cu	LS-Cu	ALS-Cu	CG-Cu	isotropic polycrystalline Cu
I(111)/ I(200)	3.85	0.75	1.84	1.0	0.12	2.13

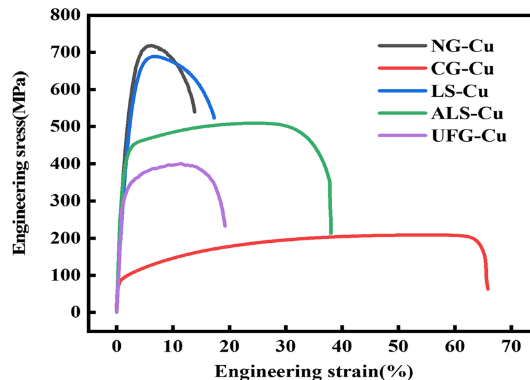

Fig. 5 The tensile test curves of the NG-Cu, UFG-Cu, LS-Cu, ALS-Cu, and CG-Cu at the strain rate of 4.17×10^{-2} s^{-1} under room temperature

monolithic UFG-CU prepared at high current density of 10 A/dm^2, the ratio (0.75) of diffraction intensity of is evidently lower than that of isotropic polycrystalline Cu, implying that the UFG-Cu shows a (200) preferred growth texture. This phenomenon that the growth texture changes with the current density has also been observed in the previous reports on nanostructured nickel under different current densities (Ref 17). For the LS-Cu that is formed by the alternate growth of the monolithic NG-Cu layer and UFG-Cu layer, the ratio (1.84) of the diffraction peak I(111)/I(200) closes to that of isotropic polycrystalline Cu, which implies a non-preferred growth orientation (i.e., a random growth). But here it should be noted that such a non-preferred growth orientation reflected by the diffraction peak intensity for the LS-Cu sample should be the result of mechanical mixing of the growth texture of the monolithic NG-Cu and that of the monolithic UFG-Cu. After heat treatment, as shown in Fig. 4, the preferred growth trend along the 200 crystal plane is obviously increased and the intensity of the (200) diffraction peak is similar to that of the (111) diffraction peak, which means that the ALS-Cu has the double preferred growth orientation along (111) crystal plane and (200) crystal plane. Combined with TEM results, the XRD results further illuminates that both the size and the preferred growth orientation of grains have evidently changed for the ALS-Cu attained by heat treatment of LS-Cu in comparison with the LS-Cu. The CG-Cu sample obtained by tempering the electrolytic Cu at 500 °C for 4 h shows a very remarkable (200) preferred growth texture with an ultralow ratio (0.12) of the diffraction intensity of the diffraction peak I(111)/I(200), which further implies that tempering can promote the preferred growth of grain along a (200) crystal plane.

Figure 5 shows the engineering stress-strain curve of the NG-Cu, CG-Cu, LS-Cu, ALS-Cu and UFG-Cu under a strain rate of 4.17×10^{-2} s^{-1} at ambient temperature. It can be seen

that the present five as-prepared Cu samples with different microstructure all exhibit an elastic–plastic deformation in tension, but their deformation behavior and mechanical properties are remarkably different. The monolithic NG-Cu exhibits an extremely high YS of about 700 MPa, which is nearly seven times higher than that (about 100 MPa) of the present CG-Cu (grain size > 20 μm) prepared by annealing the electrolyte Cu. However, unlike that the CG-Cu exhibits a very large uniform deformation ability during tension, the monolithic NG-Cu shows severe plastic instability during tension. As shown in Fig. 5, a premature rapid necking is rapidly activated when the uniform plastic deformation is only maintained at less than 2% and as a result, only a less strain 15% ETF with a large post necking strain of near 12% is attained. Such a mechanical behavior with high strength and low plasticity accompanied a premature rapid necking is in fact a typical mechanical characteristic that previous reported monolithic NG metals exhibit. The LS-Cu formed by periodically incorporating microcrystalline grains into the nanocrystal matrix exhibits a tensile deformation behavior similar to that of the monolithic NG-Cu, but the premature necking behavior for the LS-Cu in comparison with the monolithic NG-Cu is obviously delayed. As shown in Fig. 5, the necking behavior begins to occur when the uniform plastic deformation of the LS-Cu continues to close to 5% and furthermore the flow rate of uneven plastic is also significantly reduced, and as a result, a 20% ETF with a near 12% non-uniform strain accompanied by a slightly reduced YS of about 600 MPa is obtained for LS-Cu in tension. However, for ALS-Cu samples, the rapid necking deformation behavior that occurs in the monolithic NG-Cu and LS-Cu does not appear during tension, and conversely, before the necking deformation, it exhibits a significantly large uniform plastic deformation, which produces a large uniform strain (US) of nearly 30% accompanied by a post necking elongation of less than 3% for the LS-Cu. In addition to the significantly high ductility, as shown in Fig. 5, the ALS-Cu also has a relatively moderate tensile strength with a YS of about 470 MPa and UTS of about 500 MPa. For a structural material, strength and plasticity are usually contradictory, that is, low strength is often accompanied by high plasticity. Here, it can be observed from Fig. 5 that although the monolithic UFG-Cu exhibits lower tensile strength compared to the ALS-Cu, its tensile ductility is not further improved compared with that of the ALS-Cu and only an ETF of approximately 20% with a US of near 15% is obtained for the monolithic UFG-Cu. This further means that constructing such a composite structure with multi-scale grain distribution can optimize the optimal combination of material strength and plasticity.

In order to further illuminate the superior mechanical properties of the ALS-Cu, the mechanical properties involving the YS and US for homogeneous structure and heterogeneous structure Cu from the literature and the present our ALS-Cu, NG-Cu, CG-Cu, LS-Cu, UFG-Cu are summarized in Fig. 6 (Ref 2, 4, 18-24). The purple shaded area marked by the letter "I" and the green shaded area marked by the letter "II", as shown in Fig. 6, represent homogeneous structure NC Cu with grain size distribution from 72 to 320 nm and heterostructure NC Cu with broad grain size distribution, respectively. It can be seen that the homogeneous structure Cu locates at near or below of trend line, implying that the homogeneous structure exhibits high YS but disappointing US. For most heterogeneous structure specimens, the intersections of YS and US are mostly near trend lines. For example, the bimodal Cu marked by

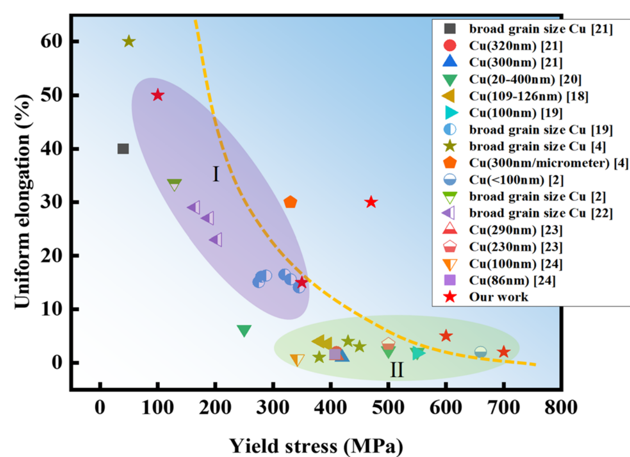

Fig. 6 Summaries of the YS and UE for the present five as-prepared Cu samples and the previous reported Cu samples with homogeneous and heterogeneous structure from the literature

orange pentagon and the gradient Cu marked by inverted green triangle exhibit a low YS at similar uniform elongation. However, it is worth noting that the bimodal structure Cu and the ALS-Cu with multimodal grain size distribution locate at away from the trend line and exhibit a large uniform elongation at a similar YS, which implies that the ALS-Cu specimens have superior work hardening ability and an optimal combination of strength and plasticity.

It is generally considered that the necking behavior of materials is related to the instability of ductility, which is considered to be attributed to the insufficient strain hardening ability. The normalized work hardening rate (WHR) ($\theta = (d\sigma_{true}/d\delta_{true})/\sigma_{true}$) is an effective index for evaluating the strain hardening ability of materials during deformation stage. So, the normalized work hardening rate for the present as-prepared Cu with different microstructure plotted as a function of true strain is shown in Fig. 7. It can be seen from Fig. 7 that the CG-Cu samples exhibit a superior strain hardening ability during the deformation process, and its normalized WHR is maintained at high level of about 50.8%. The large strain hardening ability of traditional coarse-grained metals originations from the propagation and entanglement of many dislocations inside the grains during the deformation process. Compared with the CG-Cu, the monolithic NG-Cu exhibits a disappointing strain hardening ability, as shown in Fig. 7, and the normalized WHR of the monolithic NG-Cu rapidly decreases to zero after a small true strain less than 6.9%. When the large grains of near micron size are periodically incorporated into the NC matrix, the strain hardening ability of NC copper is improved to a certain extent, as shown in Fig. 7, that the LS-Cu maintains a large strain hardening ability and a positive normalized WHR for the LS-Cu is sustained to a larger strain level of about 13.26%, which means that the incorporation of large grains is beneficial to improve the strain hardening ability of nanocrystals. For the UFG-Cu sample composed entirely of nearly micrometer-sized grains, its strain hardening rate can be maintained to the strain level of about 12.2%. It cannot be imagined that compared with LS-Cu and UFG-Cu, ALS-Cu exhibits a durable strain hardening ability, as shown in Fig. 7, and the positive normalized WHR is

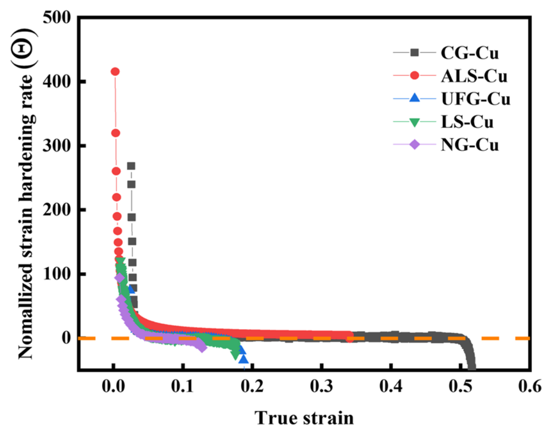

Fig. 7 The work hardening rate of the NG-Cu, UFG-Cu, LS-Cu, ALS-Cu, and CG-Cu at the strain rate of $4.17\times10^{-2}s^{-1}$

maintained at an extremely high strain level (about 30%), which is obviously consistent with the super uniform deformation ability of ALS-Cu during the tension. The above comparison results not only show that ALS-Cu samples have greater strain hardening ability, but also, more importantly, imply that the strain hardening effect given by heterostructures is not only related to the size of the incorporated large grains, but also related to the distribution of heterostructures. In the previously reported layered structures and most of bimodal structures, the incorporated large grains are often mechanically distributed in the NC matrix in the form of flakes or clusters, where the large grain region and the small grain region are actually distributed independently, and the large grain region is often separated by a wide NC region. In such a heterostructure, the effective dislocations provided by the large grains cannot coordinate the whole adjacent nanocrystalline region effectively. It can be imagined that in this case, due to the lack of coordination of dislocations provided by the large grains, some regions with insufficient strain hardening ability will exist in the internal regions of such adjacent nanocrystalline regions during deformation. At the same time, because the nanocrystalline layer in such heterostructure cannot be effectively coordinated to carry out the necessary deformation, the deformation of the heterostructure will be concentrated in these ultrafine grain regions that relatively easy to be deformed. However, for the ultrafine grain layer with a wide thickness or a large cluster area, the deformation between grains in the process of deformation lacks the necessary constraints from nanocrystals (i.e., the dislocation slip between the ultrafine grains is not hindered to maintain the necessary strain hardening), which again will lead to local uneven plastic flow. As a result, in such a heterogeneous environment, the heterostructure in fact cannot play an effective role in coordinating the strain hardening ability of materials. However, for the present multi-stage structure, we designed, as shown in Fig. 7, the produced large gains and the small grains are uniformly and randomly distributed and they are attached to each other in the interior of the multi-stage structure. It is obvious that in such a heterogeneous environment, the effective dislocations provided by the large grains can better coordinate the deformation of the neighboring nanocrystals, which improves the strain hardening ability of the nanocrystalline region. At the same time, the neighboring surrounding small nanocrystals, which are equivalent to precipitates, can also act as an effective local barrier to the motion of dislocations sourced from the large grains during deformation, which can prevent the abnormal softening and yielding of the large grain area caused by the continuous slip flow of dislocations along the large grain region and give the large grains greater hardening ability. Such mutual coordination and restriction between the large grains and small grains during deformation endow the material more durable strain hardening ability. Besides, there are more complex strain paths and strain components with very larges strain gradients under such heterogeneous environment with multi-stage distributed structure in comparison with the previously reported layered structures and bimodal. In such structural environment with a large strain gradients, an excessively large number of geometrically necessary dislocations will be forced to be present to accommodate the large strain gradient for better deformation (Ref 25). These additional coordinated dislocations can provide additional strain hardening ability for the ALS-Cu. In addition, the higher strain hardening ability for the ALS-Cu may also be attributed to the additional contribution of the double preferred growth orientation texture. In the process of plastic deformation, the dislocations slipping along the crystal planes from different preferred growth orientations will block each other and size distribution structure can regard as an effective channel to release the stress concentration by more dislocation activity provided by large-sized grains and the coordination of large grains and small grains, which makes the nucleation of microvoid difficult and avoids the premature fracture and then stabilizes the material (Ref 26-28).

The improved deformation ability for the ALS-Cu also can be further illuminated by the different surface deformation traces from these Cu samples after deformation. Figure 8 shows the captured deformation surface morphology from the region near the fracture front of CG-Cu, NG-Cu, LS-Cu, UFG-Cu and ALS-Cu after tension, and the corresponding local enlarged region marked by different letters is shown in Fig. 8(f), (g), (h), (i) and (j). It can be seen from Fig. 8(a) that CG-Cu exhibits an obvious convex and concave deformation feature and deformation surface with a large number of gill-like slip bands exhibited by white arrow was captured in Fig. 8(f), which are approximately 45 angles to the direction of the tensile axis. Moreover, these gill-like slip bands are uniformly distributed in the deformed grains with different orientation and cross and intersect at the grain boundaries. Such gill-like slip bands have been observed in previous reports, which is actually a typical deformation feature of CG metals (Ref 29). Its formation sources from the continuous slip of a large number of dislocations during deformation, which contributes to the large uniform deformation ability of CG metals. However, for the monolithic NG-Cu, as shown in Fig. 8(b), the entire deformation surface looks very planar and only the small local deformation region charactered by a few slightly grooved shear bands concentrated near the fracture was captured from the local magnification image shown in Fig. 8(g), which obviously is consistent with the observed early necking deformation behavior with very small uniform plastic strain exhibited by the NG-Cu during the tension. The periodic mechanical incorporation of large grains leads to significant changes in the morphology of the deformed surface of the NC matrix. As shown in Fig. 8c, for the LS-Cu, the deformed surface becomes obviously rougher than that of the monolithic NG-Cu, and furthermore, the deep furrow-shaped shear band with a bidirectional shear direction, which are approximately 45

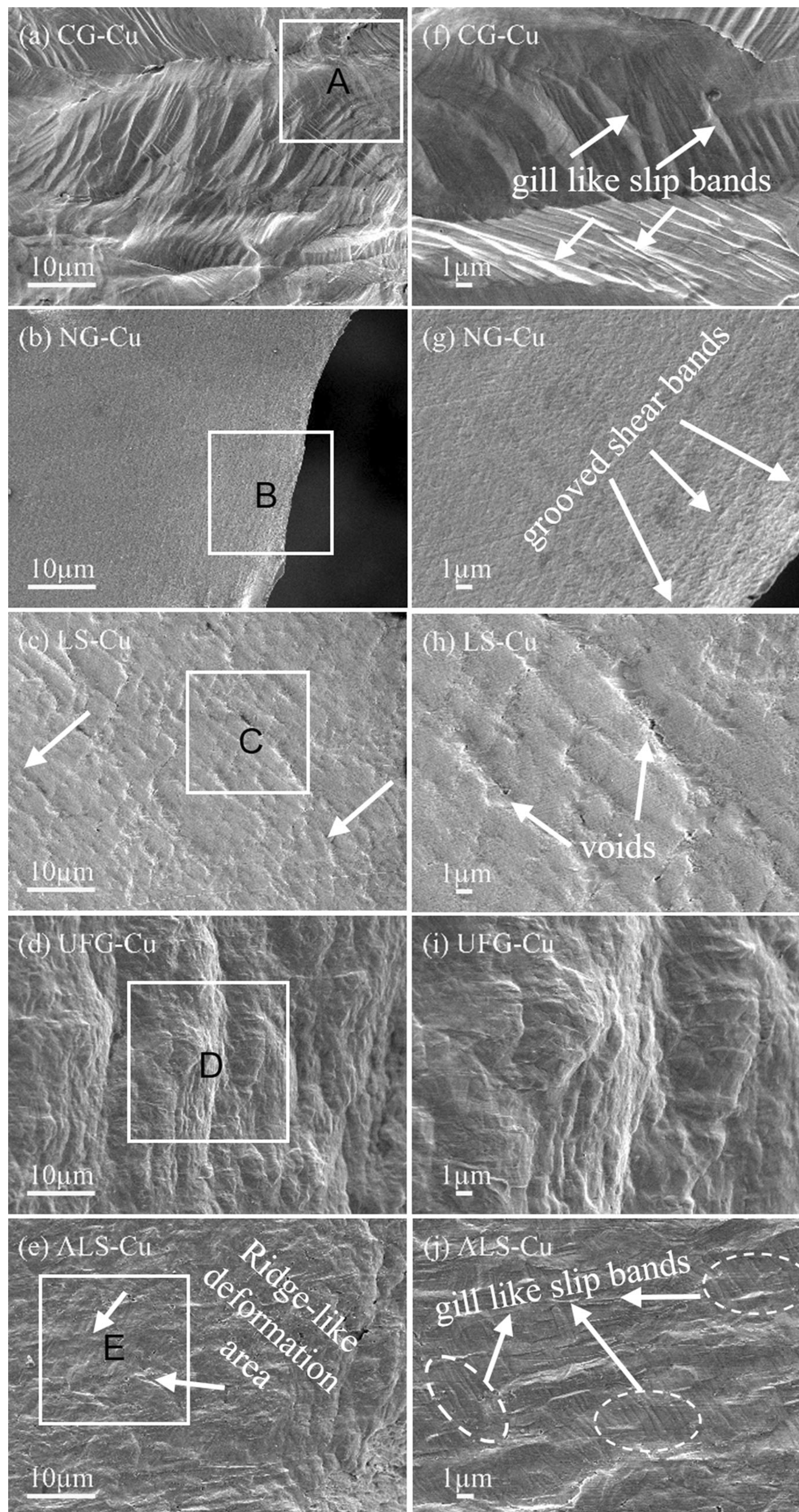

Fig. 8 The morphology of deformation surface of five as-prepared Cu samples after tension: (a) the CG-Cu and (f) the local magnification image corresponding to A region of CG-Cu; (b) the NG-Cu and (g) the local magnification image corresponding to B region of NG-Cu; (c) the LS-Cu and (h) the local magnification image corresponding to C region of LS-Cu; (d) the UFG-Cu and (i) the local magnification image corresponding to D region of UFG-Cu; (e) the ALS-Cu and (j) the local magnification image corresponding to E region of ALS-Cu

and 135 angles to the axial direction appears on the whole detected deformed surface, where some square-shaped uplift and collapse shear units formed by the intersection of these shear bands and some cavities as marked by the arrow is also observed. Similar deformation surface with such shear characteristics also was found in the recently reported layered NS Cu and Ni (Ref 5, 6). The appearance of such cross-slip bands with a bidirectional shear direction illuminates that the incorporation of large grains increases the effective dislocation activity and promotes the slip deformation. However, here, it should be emphasized that the cross-slip band induced by the mechanical incorporation of large grains into nanocrystals can improve the deformation of NC matrix to some extent, but such a cross-shear band with a specific direction is easy to cause the formation of local defects such as the above voids at the intersection of shear bands marked by the arrow shown in Fig. 8(h) in the process of maintaining material deformation, which may be the reason why the layered NS still shows a premature necking during tension. The deformed surface of the monolithic UFG-Cu shown in Fig. 8(d) has a collapse and uplift surface feature with remarkable wrinkle-shaped shear deformation bands with a direction parallel to the fracture direction form. Such deformation surface morphology characteristics mean that the monolithic UFG-Cu has undergone a large local severe inhomogeneous deformation in the region near the fracture, which is obvious consistent with the large non-uniform strain exhibited during tension. However, unlike the LS-Cu, there is no furrow-shaped cross-shear deformation bands as observed in Fig. 8(c), and as shown in Fig. 8(e), the whole fracture surface of the detected shows the deformation surface characteristics of uplift and collapse induced by the deformation, which indicates that the multi-stage structure copper has undergone greater plastic deformation than the LS-Cu. Moreover, compared with the UFG-Cu, the structural characteristics of deformation induced bulge and collapse for the ALS-Cu appear to be more flat and more uniform, which indicates that compared with UFG-Cu, the ALS-Cu undergoes a more uniform plastic deformation, which is consistent with the above tensile behavior. Moreover, it is inconceivable that many deformed regions containing dislocation slip bands similar to that exhibited on the CG deformed surface are captured from the deformed surface region of the ALS-Cu, as shown by the dotted area in Fig. 8(j). Furthermore, it can be observed that the length of these local slip bands is close to the micron scale, and these slip bands are intermittently distributed on the deformation surface. At the same time, it can also be noted from Fig. 8(e) that there are ridge-like shear deformation areas near the termination area of these slip bands, as shown by the arrow. The formation of this kind of shear band should be the result of the coordination and constraint of randomly distributed large grains and small grains in the deformation process. For the UFG-Cu or the UFG layer from the LS-Cu, the large ultrafine grains with the grain size close to nearly micron size can maintain deformation through dislocation slip during deformation, but these slip dislocations are easy to slide along a single slip direction due to the lack of effective restraint of their movement, resulting in a continuous plastic flow and eventually premature yield (Ref 30, 31). This conjecture can be confirmed by the fracture features with large necking and less dimples behind it. While in such a multi-stage structure where these large grains are surrounded by a large number of randomly distributed small grains, the slip dislocations derived from the large grains for coordinated deformation can no longer slide continuously along a certain slip direction over a large distance like that they do in homogeneous and layered structures, but slip locally in a short distance space due to the obstacles and constraints of the interface barriers provided by the surrounding small grains. In such a constrained environment, the continuous plastic flow like that occurs in the large grain region in the homogeneous and layered structure will be effectively restrained in the plastic deformation process of multistage copper. At the same time, in such a constrained space, new dislocation slip activities on different slip planes and on the same slip plane will be continuously activated driven by the stress gradient induced by multistage structure to coordinate the plastic deformation in this local space. In this way, effective dislocations from the same slip plane or different slip systems will continue to slip and pile up in this confined space formed by this multi-stage structure, eventually leading to the formation of gill-like shear bands similar to that of CG in the space spanning about one to two grains. Obviously, the randomly distributed regional shear slip bands formed by the mutual restraint of large and small grains can effectively coordinate the local deformation and bring a more stable and continuous strain hardening ability to the ALS-Cu in the process of plastic deformation and contribute a larger uniform plastic deformation.

The fracture morphologies of NS Cu samples with different microstructure are also compared to further illustrate the advantages of the multimodal size distribution in optimizing the deformation ability of materials. The fracture morphologies of NG-Cu, LS-Cu and ALS-Cu samples are shown in Fig. 9, and the corresponding local magnification images marked by the letter "A," "B" and "C" are also shown in Fig. 9(d), (e) and (f). It can be seen from Fig. 9(a) that the monolithic NG-Cu exhibits an uneven fracture with obvious characteristics of double dimples, where some rod-shaped dimples marked by white arrow are intermittently distributed on the matrix with very fine and shallow dimples. It can be roughly seen from the enlarged illustration in Fig. 9(a) that the diameter of the shallow dimple structure is in the range of 100-200 nm, while that of the embedded rod-shaped dimple is in the range of 0.5-2 μm. The small and obvious dimple structure of nanocrystals means that the fracture process of nanocrystals starts after a small deformation. Such features with bimodal dimple size distribution have also been observed in the uniform nanocrystalline nickel that we recently reported (Ref 5, 6). Recent studies have suggested that for nanocrystals, dimples are also formed by the expansion and coalescence of micropores, similar to the traditional coarse grains (Ref 32, 33). However, due to the lack of effective dislocations in fine nanocrystals, the nucleation of micropores is no longer formed by transgranular dislocations as in coarse grains, but by stress concentration at grain boundaries. Driven by this kind of stress concentration, the micropores propagate along the grain boundary and across the space area larger than the grain size and merge with the neighboring micropores to open the shear fracture. Depending on this process, the dimple structure of nanocrystals is often tens of times of its own grain size. As a result, the size of the dimple structure of nanocrystals is often tens of times larger than that of their own grains in NG-Cu. The fracture characteristics of the large dimple structure intermittently distributed in the small and shallow dimple structure matrix show that the stress concentration formed in the NC matrix during deformation is uneven, and the large abnormal stress concentration is formed in many areas due to the lack of

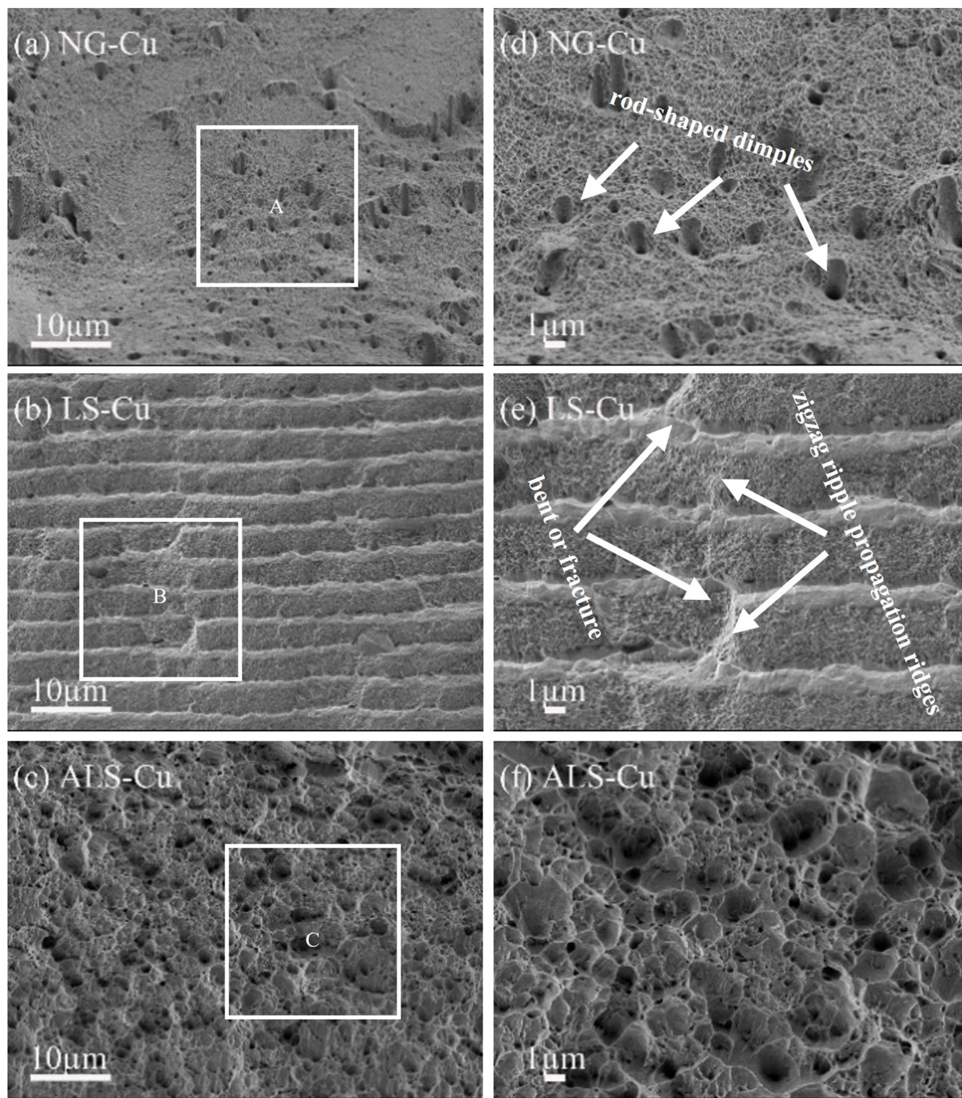

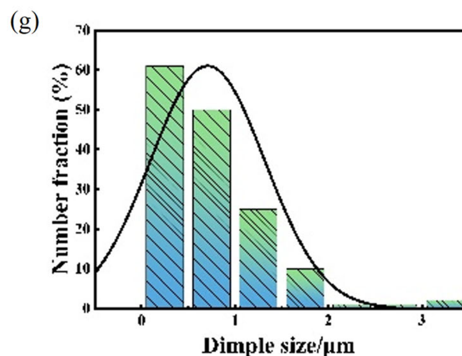

Fig. 9 The fracture morphology of five as-prepared Cu samples after tension: (a) The NG-Cu and (d) the corresponding local magnification image of A region marked by the white box in the NG-Cu; (b) The LS-Cu and (e) the corresponding local magnification image of B region marked by the white box in the NG-Cu; (c) The ALS-Cu and (f) the corresponding local magnification image of C region marked by the white box in the ALS-Cu and (g) the simple size distribution image of the ALS-Cu

dislocation coordination deformation, which may cause the premature yield and instability of the NG-Cu.

For the LS-Cu, a very significant fracture with alternating fracture characteristics, where a relatively flat fracture area with a concave surface of about 3 μm in thickness and a relatively raised fracture area with a surface of about 1 μm in thickness alternates along the radial direction of the fracture, are captured. Obviously, the alternating fracture characteristics are very

consistent with our layered structure. It can be clearly seen from Fig. 9(b) that the fracture area corresponding to the NC layer in the layered structure does not show the characteristics of double dimple structure, but presents a finer and shallower dimple structure with the size of 200-300 nm. There are no large abnormal dimples in the fracture zone of nanocrystals in the layered structure, which indicates that the periodic incorporation of micron-sized large grains increases dislocation activity, reduces the stress concentration in the NC region, and avoids the occurrence of abnormal stress concentration, so that the formation of dimples is driven by relatively uniform small stress concentration, which leads to the formation of finer and more uniform dimples. However, the fracture area corresponding to the large grain layer does not show typical dimple structure fracture characteristics, but presents a ridge-like fracture characteristics. The ridge-like fracture features reflect that the ultrafine grain layer sandwiched between the NC layers undergoes a large non-uniform plastic deformation during the deformation process of layered copper. In other words, the plastic deformation of the layered structure is mainly concentrated in the deformable ultrafine grain layer, while the NC layer experiences less deformation, which may be why the dimple size of the NC layer in the layered structure is obviously smaller than that of the homogeneous nanocrystalline. At the same time, from the fracture surface, we can also observe some zigzag ripple propagation ridges formed by crack propagation across the NC layer and large grain layer in Fig. 9(e), as shown by the arrow. Such crack propagation characteristics imply that in the deformation process of such layered structure, in addition to the limited dislocations sliding along the axial direction in their respective layers to coordinate the deformation, some dislocations will also change the slip direction and expand along the radial direction to coordinate and maintain the necessary deformation driven by the shear stress, which should be observed from the deformation surface of the layered structure mentioned above the reason for the formation of cross-slip band. In addition, as shown by the arrow in Fig. 9(e), the ultrafine grain layer is obviously bent or fractured as the crack propagates along the radial direction through the ultrafine grain layer, which is also consistent with the surface bulge, collapse and cavity characteristics of the cross-slip band observed on the surface. Furthermore, it can be further implied from the characteristics of layered fracture that the mechanically incorporated large grains can contribute more deformation ability to the nano-matrix in the deformation process of this kind of lamellar structure, but at the same time, this kind of large grain layer also becomes the weakest link in the deformation process of this kind of layered structure (i.e., shear flow yield and voids preferentially formed area). Once it exceeds the flow stress that the UFG layer can bear, dislocations will continue to propagate, which will lead to premature plastic instability similar to that exhibited by NG-Cu. This may be the reason why the ability of uniform plastic deformation of the layered copper is not significantly improved during deformation. However, the fracture morphology of ALS-Cu with multimodal grain size is in sharp contrast with that of the layered template. As shown in Fig. 9(c), on the fracture surface of this kind of multi-stage structure copper with large and small grains randomly distributed, there is no fracture characteristic composed of ridge structure and dimple structure as shown on the fracture surface of layered structure, on the contrary, a fracture completely composed of dimple structure with wide dimple size distribution where the dimples with different grain size are randomly distributed to each other is presented in Fig. 9(f). Based on the quantitative statistics from different fracture areas, as shown in Fig. 9(g), the size of dimple structure on multi-stage structure copper fracture is in the range from tens of nanometers to nearly 3.5 μm. The fracture characteristics of the dimple structure with wide size distribution obviously correspond to the microstructure of ALS-Cu composed of multi-stage grains. The transition of fracture characteristics from ridge type and dimple type mixed fracture to all dimple type fracture not only means the change of fracture behavior of incorporated large grains, but also implies that the distribution of large grains and small grains has a great influence on the micro-fracture process of materials. In the layered structure environment, because the large grain layer with a certain thickness is intermittently incorporated into the hard nanocrystals, the deformation of the layered structure will be coordinated preferentially by the plastic deformation of the large grain layer which is easy to deform. However, in the process of plastic deformation, due to the lack of effective constraint on dislocation slip in the large grain layer mechanically embedded into the NC matrix (i.e., the large grain layer cannot form effective strain hardening during plastic deformation.), the dislocation sliding continuously along a certain direction under the driving of shear force will cause serious local plastic flow in the local area of the large grain layer, and finally, shear fracture occurs in the local plastic flow area under the action of pure shear force companied by the formation of a ridge-like fracture region. However, for NS Cu with multi-stage structure, due that the large grains and small grains are randomly distributed in the matrix and fused with each other, the dislocations in large grains no longer slip along the determined slip direction under the action of shear stress, but only slip locally under the action of shear stress, and then accumulate at the interface between them. Obviously, under such interfacial constraints, the local plastic flow caused by dislocation slip will be effectively restrained, which makes the fracture of large grains no longer proceed in the pure shear mode caused by plastic flow as in the layered structure, but in the way of micropore growth and expansion induced by the local stress concentration formed by the accumulation of slip dislocations at the grain boundary. In other words, due to the effective constraint of randomly distributed small grains, the fracture mechanism of the large grain area in the multi-stage structure copper is transformed into a microporous aggregation fracture mechanism, which leads to the observation of a randomly distributed large dimple on the fracture surface of multi-stage structure copper. In addition, it can also be noted that the dimples on the fracture surface of multi-stage structure copper have deeper pores in both large and small dimples than those of uniform and layered structure copper. This dimple with deeper holes means that the multi-stage structure copper experienced greater plastic deformation during the deformation process before fracture (i.e., in the formation of dimple structure), which is also obviously consistent with the larger plastic deformation of the multi-stage structure copper during the tensile process (Ref 34). In such a multi-stage structure, the effective coordination of large grains randomly distributed in the matrix can greatly reduce the stress concentration in the interface region, which can not only delay the formation of

micropores, but also reduce the nucleation point of micropores. At the same time, it can also be imagined that once these micropores are formed, under the coordinated deformation of such multi-stage structure, they will grow gradually through effective dislocation sliding driven by smaller internal stress, and merge with the nearby micropores, which may lead to a deeper dimple structure in multi-stage structure copper. Obviously, the comparison of fracture characteristics further shows that the multi-stage structure designed at present has a great advantage in controlling the plastic deformation of materials compared with uniform structure and layered structure.

4. Conclusion

In summary, a bulk NS Cu with a multimodal grain size distribution spanning from 30 nm to 1.12 μm where the large-sized grains and the small grains are randomly distributed with each other was successfully prepared by annealing a pre-designed Cu template with a layered structure fabricated by electrodeposition. In comparison with previously reported NS Cu with homogeneous and heterogeneous structure, the present NS Cu with a random distribution of multimodal grain size exhibits a larger and more durable strain hardening ability during tensile deformation, which produces a superior combination of high ductility with the elongation to failure of near 40% and moderated strength with the ultimate tensile strength of about 500 MPa. Compared with homogeneous and other heterogeneous NS Cu, the improved ductility and strain hardening ability for the present NS Cu can be attributed to the additional strengthening effects induced by this multistage structure induces during the plastic deformation, including producing more effective coordinated deformation dislocation activity, inhibiting the occurrence of the local plastic flow and effectively releasing the local stress concentration. Such multistage structure changes the shear slip mechanism of NS Cu. A transition from the grooved slip band parallel to the fracture direction for the NS Cu with uniform narrow grain size distribution to the cross-shear deformation band with double shear direction for the NS Cu with alternate distribution of nc layer and UFG layer then to the composite slip shear deformation mode charactered by the gill-like shear bands companied by ridge-like shear deformation area for the present NS Cu with a random distribution of multimodal grain size in the shear slip band mode is captured from the surface deformation region of these structures. In addition, such multi-stage structure changes the fracture behavior of NS Cu. An obvious transition from a double dimple fracture behavior for the NG-Cu to an alternating fracture behavior for the LS-Cu to a randomly distributed dimple of large dimples and small dimples fracture behavior for the ALS-Cu is observed from the fracture of these structures. The present work provides a new strategy for more flexible design of heterogeneous structures with a random distribution of multimodal grain size to improve the mechanical properties of NS materials.

Acknowledgments

This work was financially supported by National Natural Science Foundation of China (Nos. 21673135 and 21972090) and Science and Technology Commission of Shanghai Municipality (Nos. 17020500700, 18511110902 and 19DZ2271100).

References

1. L. Kurmanaeva, H. Bahmanpour, T. Holland, J. McCrea, J.H. Lee, J. Jian, H. Wang, E.J. Lavernia and A.K. Mukherjee, Room Temperature Mechanical Behaviour of a Ni-Fe Multi-layered Material with Modulated Grain Size Distribution, *Philos. Mag. Lett.*, 2014, **94**(31), p 3549–3559
2. Y.M. Wang, M.W. Chen, F.H. Zhou and E. Ma, High Tensile Ductility in a Nanostructured Metal, *Nature*, 2002, **419**(31), p 912–914
3. T. Mineta, T. Saito, T. Yoshihara and H. Sato, Structure and Mechanical Properties of Nanocrystalline Silver Prepared by Spark Plasma Sintering, *Mater. Sci. Eng. A*, 2019, **754**, p 258–264
4. T.H. Fang, W.L. Li, N.R. Tao and K. Lu, Revealing Extraordinary Intrinsic Tensile Plasticity in Gradient Nano-grained Copper, *Science*, 2011, **331**, p 1587
5. X.X. Shen, M. Wu, D.M. Ji, Q.J. Xu and D.H. Cheng, The Mechanical Behavior of a Layered Nanostructured Ni with an Alternating Growth of Ultrafine Grains and Nano-sized Grains Fabricated by Electrodeposition, *Mater. Sci. Eng. A*, 2018, **713**, p 43–51
6. B. Zheng, X.X. Shen, H.S. Jiao, Q.J. Xu and D.H. Cheng, Enhanced Mechanical Properties of Multilayered Cu with Modulated Grain Size Distribution, *Adv. Eng. Mater*, 2017, **20**, p 1700849
7. N.P. Wasekar, P. Haridoss, S.K. Seshadri and G. Sundararajan, Influence of Mode of Electrodeposition, Current Density and Saccharin on the Microstructure and Hardness of Electrodeposited Nanocrystalline Nickel Coatings, *Surf. Coat. Technol.*, 2016, **291**, p 130–140
8. D. Grujicic and B. Pesic, Electrodeposition of Copper: The Nucleation Mechanisms, *Electrochim. Acta*, 2002, **47**, p 2901–2912
9. T. Yamamoto, K. Igawa, H. Tang, C.Y. Chen, T.M. Chang, T. Nagoshi, O. Kudoc, R. Maeda and M. Sone, Effects of Current Density on Mechanical Properties of Electroplated Nickel with High Speed Sulfamate Bath, *Microelectron. Eng.*, 2019, **213**, p 18–23
10. J.V.T. Kumara, S. Jayaprakasama, K.A. Padmanabhan, A.A. Misochenkob and V.V. Stolyarov, On the Tensile Behaviour of Coarse and Ultrafine Grained NiTi, *Mater. Charact.*, 2019, **149**, p 41–51
11. Z.T. Bai, G.H. Balbus, D.S. Gianol and Y. Fan, Mapping the Kinetic Evolution of Metastable Grain Boundaries Under Non-equilibrium Processing, *Acta Mater.*, 2020, **200**, p 328–337
12. Z.Y. Ren, R. Ma, G.C. Hu, J. Wu, Z.H. Wang and C. Luo, Grain Refinement and Mechanical Response of U-5.5 wt%Nb Alloy Produced by Cold Rolling and Heat Treatment, *J. Nucl. Mater.*, 2017, **494**, p 72–78
13. Q.Y. He, T.L. Huang, L.F. Shuai, Y. Zhang, G.L. Wu, X.X. Huang and D.J. Jensen, In-Situ Investigation of the Evolution of Annealing Twins in High Purity Aluminium, *Scr. Mater.*, 2018, **153**, p 68–72
14. Z.H. Cao, L.J. Xu, W. Sun, J. Shi, M.Z. Wei, G.J. Pan, X.B. Yang, J.W. Zhao and X.K. Meng, Size Dependence and Associated Formation Mechanism of Multiple-Fold Annealing Twins in Nanocrystalline Cu, *Acta. Mater.*, 2015, **95**, p 312–323
15. S. Dash and N. Browns, An Investigation of the Origin and Growth of Annealing Twins, *Acta Mater.*, 1963, **11**, p 1067–1075
16. C.H. Tseng and C. Chen, Growth of Highly (111)-Oriented Nanotwinned Cu with the Addition of Sulfuric Acid in $CuSO_4$ Based Electrolyte, *Cryst. Growth Des.*, 2019, **19**, p 81–89
17. N.P.W.P. Haridoss, S.K. Seshadri and G. Sundararajan, Influence of Mode of Electrodeposition, Current Density and Saccharin on the Microstructure and Hardness of Electrodeposited Nanocrystalline Nickel Coatings, *Surf. Coat. Technol.*, 2016, **291**, p 130–140
18. Y.P. Wang, R.D. Fu, X.Y. Zhou, G.B. Thompson, Z.Z. Yu and Y.J. Li, *Mater. Lett.*, 2016, **185**, p 546–549
19. C.X. Huang, Y.F. Wang, X.L. Ma, S. Yin, H.W. Höppel, M. Göken, X.L. Wu, H.J. Gao and Y.T. Zhu, Interface Affected Zone for Optimal Strength and Ductility in Heterogeneous Laminate, *Mater. Today*, 2018, **21**, p 713–719
20. G.Y. Wang, Z.H. Jiang, Q. Jiang and J.S. Lian, Mechanical Behavior of an Electrodeposited Nanostructured Cu with a Mixture of Nanocrystalline Grains and Nanoscale Growth Twins in Submicrometer Grains, *J. Appl. Phys.,* 2008, **104**, p 084305

21. S.Z. Han and M. Goto, Jee-Hyuk Ahn, Sung Hwan Lim, Sangshik Kim, Jehyun Lee, Grain growth in ultrafine grain sized copper during cyclic deformation, *J. Alloys. Compd.*, 2014, **615**, p S587–S589
22. Z. Yin, X.C. Yang, X.L. Ma, J. Moering, J. Yang, Y.L. Gong, Y.T. Zhu and X.K. Zhu, Strength and Ductility of Gradient Structured Copper Obtained by Surface Mechanical Attrition Treatment, *Mater. Des.*, 2016, **105**, p 89–95
23. B.Y.H. Zhao, J.F. Bingert, X.Z. Liao, B.-Z. Cui, K. Han, A.V. Sergueeva, A.K. Mukherjee, R.Z. Valiev, T.G. Langdon and Y.T. Zhu, Simultaneously Increasing the Ductility and Strength of Ultra-Fine-grained pure copper, *Adv. Mater.*, 2006, **18**, p 2949–2953
24. F. Dalla Torre, R. Lapovok, J. Sandlin, P.F. Thomson, C.H.J. Davies and E.V. Pereloma, Microstructures and Properties of Copper Processed by Equal Channel Angular Extrusion for 1–16 Passes, *Acta Mater.*, 2004, **52**, p 4819–4832
25. L.G. Sun, G. Wu, Q. Wang and J. Lu, Nanostructural Metallic Materials: Structures and Mechanical Properties, *Mater. Today*, 2020, **38**, p 114–135
26. G. Liu, Y.Q. Yang, X. Luo, B. Huang, Z.D. Kou and P.T. Li, Improving the Mechanical Properties of Titanium Films by Texture Strengthening, *Mater. Charact.*, 2017, **127**, p 365–370
27. X.D. Song, F. Wang, D.S. Qian and L. Hua, Tailoring the Residual Stress and Mechanical Properties by Electroshocking Treatment in Cold Rolled M50 Steel, *Mater. Sci. Eng. A*, 2020, **780**, p 139171
28. Y.F. Wang, C.X. Huang, Q. He, F.J. Guo, M.S. Wang, L.Y. Song and Y.T. Zhu, Heterostructure INDUCED DISPERSIVE SHEAR BANDS in Heterostructured Cu, *Scr. Mater.*, 2019, **170**, p 76–80
29. H.Z. Zhang, Z.H. Jiang, J.S. Lian and Q. Jiang, Strain Rate Dependence of Tensile Ductility in an Electrodeposited Cu with Ultrafine Grain Size, *Mater. Sci. Eng. A*, 2008, **479**, p 136–141
30. Y.T. Zhu, K. Ameyama, P.M. Anderson, I.J. Beyerlein, H.J. Gao, H.S. Kim, E. Lavernia, S. Mathaudhu, H. Mughrabi, R.O. Ritchie, N. Tsuji, X.Y. Zhang and X.L. Wu, Heterostructured Materials: Superior Properties from Hetero-Zone Interaction, *Mater. Res. Lett.*, 2021, **9**, p 1–31
31. Y. Ma, M.X. Yang, F.P. Yuan and X.L. Wu, A Review on Heterogeneous Nanostructures: A Strategy for Superior Mechanical Properties in Metals, *Met.,* 2019, **9**, p 598
32. X.X. Shen, J.S. Lian, Q. Jiang and Z.H. Jiang, The Optimal Grain Sized Nanocrystalline Ni with High Strength and Good Ductility Fabricated by a Direct Current Electrodeposition, *Adv. Eng. Mater.*, 2008, **10**, p 539–546
33. H.Q. Li and F. Ebrahimi, Ductile-to-Brittle Transition in Nanocrystalline Metals, *Adv. Mater.*, 2005, **17**, p 1969–1972
34. R. Schuhab and A. Pippana, Hohenwarter, Tailoring Bimodal Grain Size Structures in Nanocrystalline Compositionally Complex Alloys to Improve Ductility, *Mater. Sci. Eng. A*, 2019, **748**, p 379–385

Publisher's Note Springer Nature remains neutral with regard to jurisdictional claims in published maps and institutional affiliations.